Journal of
Materials Chemistry C
Materials for optical and electronic devices
www.rsc.org/materialsC

Volume 1 | Number 1 | Jan 2013 | Pages 1–100

ROYAL SOCIETY
OF CHEMISTRY

www.rsc.org/materialsC

Eco-friendly, solution-processed In-W-O thin films and their applications in low-voltage, high-performance transistors

Ao Liu,[1,2,3] Guoxia Liu,[1,2,3*] Huihui Zhu,[1,2,3] Byoungchul Shin,[4] Elvira Fortunato,[5] Rodrigo Martins[5] and Fukai Shan[1,2,3*]

[1]College of Physics, Qingdao University, Qingdao 266071, China
[2]College of Electronic and Information Engineering, Qingdao University, Qingdao 266071, China
[3]Lab of New Fiber Materials and Modern Textile, Growing Base for State Key Laboratory, Qingdao University, Qingdao 266071, China
[4]Electronic Ceramics Center, DongEui University, Busan 614-714, Korea
[5]Department of Materials Science/CENIMAT-I3N, Faculty of Sciences and Technology, New University of Lisbon and CEMOP-UNINOVA, Campus de Caparica, 2829-516 Caparica, Portugal

Abstract: In this study, amorphous indium-tungsten oxide (IWO) semiconductor thin films were prepared by an eco-friendly spin-coating process using ethanol and water as solvents. The electrical properties of IWO thin-film transistors (TFTs), together with the structural and morphological characteristics of IWO thin films, were systematically investigated as functions of the tungsten concentration and annealing temperature. The optimized IWO channel layer was then integrated on aqueous aluminum oxide (AlO_x) gate dielectric. It is observed that the solution-processed IWO/AlO_x TFT represents high stability and improved characteristics, such as an on/off current ratio of 5×10^7, a field-effect mobility of 15.3 cm^2/Vs, a small subthreshold slope of 68 mV/dec, and a threshold voltage shift of 0.15 V under bias stress for 2 h. The IWO/AlO_x TFT could be operated at a low voltage of 2 V, which was 15 times lower than that of conventional SiO_2-based devices. The solution-processable IWO thin films synthesized in a green route would be a promising candidate for large-area and high-performance application in low-cost devices.

---

* Corresponding author: gxliu@qdu.edu.cn; fukaishan@yahoo.com

1. Introduction

In the past decade, oxide thin-film transistors (TFTs) have attracted considerable attention because of their superior material properties, including their high transparency, high field-effect mobility, and high environmental stability compared to conventional amorphous silicon (a-Si:H) and organic TFT devices.[1-3] Since the first report of amorphous InGaZnO as channel material by Nomura *et al.*,[3] it has been widely studied for TFT applications due to its high mobility, low-temperature fabrication process, and applicability to large-area production characteristics. However, acid-soluble Ga_2O_3 and ZnO components in InGaZnO thin film is sensitive to wet etching processes.[4] Therefore, it is necessary to optimize the device structure in order to minimize the damage to the back channel surface of the InGaZnO active layer when etching the source and drain electrodes.[5] By contrast, Tsukagoshi *et al.* recently proposed a novel W-doped In_2O_3 (IWO) semiconductor system by sputtering technique at low temperatures (<150 ^{o}C).[4, 6] Compared to acid-soluble Ga_2O_3 and ZnO components, WO_3 is insoluble in acids except for hydrogen fluoride solutions, which can minimize the damage to the channel surface during the wet etching process. To date, IWO thin films have been used as transparent conductive oxides[7, 8], electrodes for organic light-emitting diodes,[9] anodes for organic solar cells,[10] and most recently, channel layers for oxide TFTs.[4, 6] However, all these functional IWO thin films were manufactured by vacuum-based techniques such as magnetron sputtering and pulse laser deposition, which pose the limitation in the realization of low-cost and large-area electronics. Since cost is a primary consideration in many emerging electronic device applications, such as disposable and wearable electronics. In these applications, the research based on solution process is attractive for further development and application of IWO thin films. Additionally, the solution process is possible to tune the oxide composition by simply changing the composition of the precursor solution in a straightforward and comprehensive fashion.

The keywords for next-generation display are "high performance", "eco-friendliness", and "innovative design". To achieve high-performance oxide TFTs at low temperatures (<300 ^{o}C), various novel solution processes have been proposed, such as hydrolysis,[11] combustion,[12] microwave annealing,[13] and physicochemical technique.[14] However, toxic organic solvents, e.g. 2-methoxyethanol (2-ME) and methoxyisopropanol, are toxic to human being and harmful to the environment.

Therefore, in our recent report, an eco-friendly water-inducement route was employed to fabricate the metal-oxide thin films and the fully water-induced (WI) oxide TFTs were integrated.[15, 16] For WI precursor solution, metal nitrates and de-ionized (DI) water are used as the source materials. However, the limitation of water-inducement route is that not all of the metal salts can be dissolved in water well, such as metal chlorides or acetylacetonate. To prepare the WO_3 component in soluble IWO thin film, the tungsten chloride (WCl_6) was selected as the precursor solute because of its good solubility in ethanol (another eco-friendly solvent). Eliminating the utilization of toxic solvents in IWO coating process, the eco-friendly solution-processed IWO thin film could be a promising candidate of the TFT channel.

In oxide TFTs, the gate dielectric plays a critical role in determining the electrical performance. The application of high-k gate dielectric could generally bring about an improvement in electrical performance, especially for the field-effect mobility (μ_{FE}), by forming an excellent heterogeneous interface with semiconductor channel layer.[17-19] In the past decade, several research groups have conducted the studies using solution-processed high-k dielectrics, such as Al_2O_3,[20] HfO_2,[21] ZrO_2,[22] and Y_2O_3[23] because the use of inorganic high-k dielectrics enables a low leakage current, through the use of a thicker film, as well as a low-voltage operation. Among various high-k dielectrics, AlO_x has been studied most extensively because of its high conduction band offset,[24] low interface trap density,[25] and its high chemical stability.[18] However, the high processing temperature and the dependency on toxic organic precursor undoubtedly limit its practical application in solution-based electronic industry.[26-28]

In this report, we demonstrate an eco-friendly solution process for the fabrication of amorphous IWO thin films and the TFT devices at low temperatures. The electrical properties of the IWO TFTs, together with the physical properties of the IWO thin films, were investigated as functions of W concentration and annealing temperature. It is found that the IWO TFTs were active at the annealing temperature as low as 240 °C, which is independent of W concentration. Bias stress measurements indicate that the IWO TFTs with higher W concentration exhibit an improved electrical stability and a reduced threshold voltage shift. Moreover, to explore the feasibility of low-voltage IWO TFT, the device was further optimized by employing the WI AlO_x thin film as

the gate dielectric. By replacing SiO_2 with the WI AlO_x dielectric film, the carrier mobilities were enhanced by a factor of 4.5 and the operating voltage was decreased from 30 V to 2 V.

2. Experimental

2.1 Precursor Solution Preparation and Characterization. The preparation details for WI In_2O_3 precursor solution can be found in our previous report.[16] The tungsten chloride (WCl_6) was dissolved in ethanol and allowed to stir overnight to form a 10 mg/mL WO_3 precursor solution. The IWO precursor solutions were prepared by adding WO_3 precursor into the In_2O_3 precursor solution so as to achieve a WO_3 weight fraction of 1%, 3%, and 5%. Here after, the IWO precursor solution with the W concentration of 1%, 3%, and 5% are abbreviated as IWO-1, IWO-3, and IWO-5, respectively. The aluminum nitrate nonahydrate ($Al(NO_3)_3 \cdot 9H_2O$) was dissolved in DI water to prepare AlO_x precursor solution. The thermal behaviors of the IWO xerogel with various W concentrations were measured using a thermal-gravimetric analyzer (TGA, Pyris1).

2.2 Device Fabrication and Electrical Characteristics. Heavily doped p-type Si substrates with a 200-nm-thick thermal SiO_2 layer were sonicated with acetone, ethanol, and DI water in sequence and dried with N_2 stream, followed by oxygen plasma treatment for 5 min. Each IWO precursor solution was filtered through 0.2 μm syringe filter and spin-coated SiO_2/p^+-Si substrates at 4500 rpm for 20 s. The thin films were then annealed at temperatures ranging from 240 ^{o}C to 330 ^{o}C for 1 h. For the fully solution-processed IWO/AlO_x TFTs, the AlO_x precursor solution was spun onto p^+-Si substrates at 5000 rpm for 20 s and baked at 150 °C for 10 min subsequently. The samples were then annealed at 350 °C for 2 h. The IWO-3 precursor solution was then spun on AlO_x/p^+-Si substrate and the laminated thin films were annealed at 300 °C for 1 h. Finally, Al source and drain electrodes were deposited by thermal evaporation through a shadow mask. To eliminate mobility overestimation, the channel length and width of the TFTs were 100 and 1000 μm, respectively. For the metal-insulator-semiconductor (MIS) device, Al/AlO_x/p^+-Si capacitors were fabricated to measure the electrical and dielectric properties of the WI AlO_x thin films. The electrical properties of AlO_x capacitors, as well as the TFT devices, were measured by using a Keithley 2634B semiconductor parameter analyzer.

The capacitance-frequency (C-f) curve of AlO_x capacitor was measured using an Agilent 4294A. The saturation mobility (μ_{sat}) was extracted from transfer characteristics using the following equation:[29]

$$I_{DS} = \left(\frac{1}{2}\frac{W}{L}C_i\mu_{sat}\right)(V_G - V_{TH})^2 \qquad (1)$$

where C_i is the areal capacitance of the gate dielectric; W and L are the channel width and length of the TFT, respectively; V_{TH} is the threshold voltage, which can be determined in the saturation region by linear fitting $I_D^{1/2}$ vs V_G plot. The density of interface states (N_s^{max}) of the TFT was calculated using the following formula:[30]

$$N_s^{max} = \left[\frac{SS \times \log e}{kT/q} - 1\right]\frac{C_i}{q} \qquad (2)$$

where k is Boltzmann constant, q is electron charge, e is base of natural logarithm, SS is the subthreshold swing, which is extracted from the linear portion of a plot of the log I_D vs V_G.

2.3 Oxide Film Characterization. The crystal structures of the IWO thin films and the WI AlO_x thin films were investigated by X-ray diffractometer (XRD, X'Pert-PRO MPD and MRD, PANalytical, Holland) with a Cu$K\alpha$1 radiation. The corresponding surface morphologies were measured by using an atomic force microscope (AFM, SPA-400, Seiko).

3. Results and discussions

To achieve high-mobility and high-stability In_2O_3-based oxide TFTs, a proper carrier-suppressing dopant should be chosen carefully. Many studies have postulated that metal ion electronegativity (χ_z) plays an important role in determining the amount of charge carriers in oxide films.[31-33] However, several reports claimed that lower χ_z is desired; while others argued that larger value of χ_z would control the oxygen vacancies better. One reason that χ_z is a poor metric to rationalize charge mobility in these systems is that it does not account for local environment.[34] Instead, Wen $et\ al.$[35] proposed an empirical relation associated χ_z with ionic radii (r), effective charge (Z) of dopant and defined a function as a scale for strength of Lewis acid (L). A stronger Lewis acid will easily accept more electrons than a weaker one. Meanwhile, a high L dopant can polarize the charge carriers away from the oxygen 2p valance band, resulting in the screening of the charges and the weakening the effect as a scattering

center, hence increasing the mobility. The equation for the classification is derived from plotting Z/r^2 against χ_z.[36]

$$L = Z/r^2 - 7.7\chi_z + 8.0 \qquad (3)$$

Among various carrier-suppressing dopants, W^{6+} was found to have a large L value (~3.16), as shown in Fig. 1. For this reason, the addition of W into In_2O_3 host will be effective to reduce the excess carriers in the film and maintain the μ_{FE} in a relatively high level.
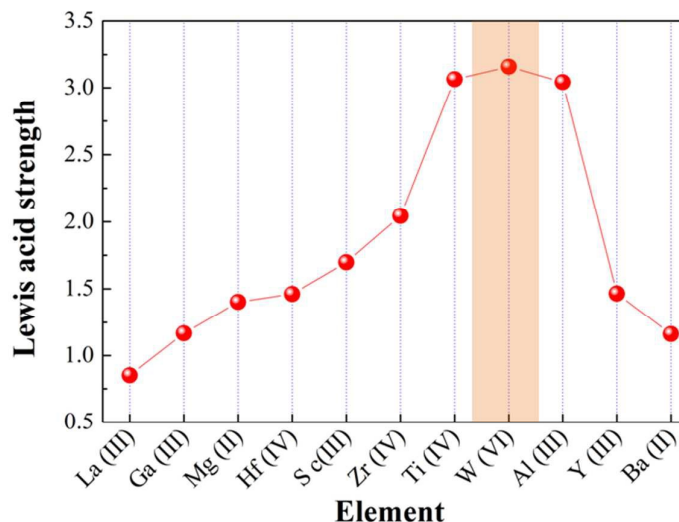
Fig. 1 Lewis acid strength values of various carrier-suppressing dopants.
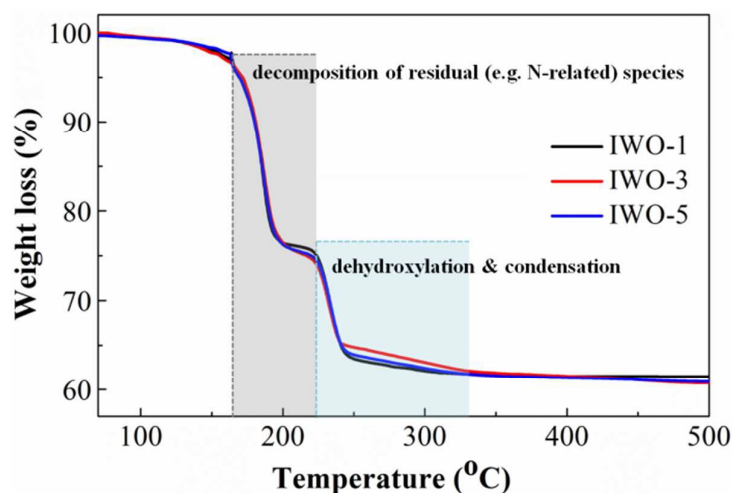
Fig. 2 TGA curves of IWO xerogel with various W concentrations.

To characterize the thermal behaviors of the IWO xerogel as a function of W concentration, TGA analyses were performed and the results are shown in Fig. 2. The IWO xerogel with various W concentrations exhibited similar thermal behavior.

Above 160 ^{o}C, two steps of weight loss were observed. The first step indicated the evaporation of volatile nitrate precursor and the thermal decomposition of the residual species.[37] The second step at higher temperature indicated the dehydroxylation and the condensation reaction. No significant weight loss was observed above 330 °C, implying that the dehydroxylation and alloy reaction were almost completed during annealing at 330 °C. Therefore, sufficient thermal energy can be provided to form IWO semiconductor thin films from the precursor solutions at 330 ^{o}C.

It is known that the carrier concentration and transport properties of the metal-oxide thin films from molecular precursor solutions are strongly dependent on the annealing temperature and on the metal composition.[15, 19, 31-33] Generally, to explore a new emerging channel component in TFTs, thermally-grown SiO_2 is adopted as the dielectric because of its high reliability, low trap defects, and smooth surface. In this report, the IWO precursor solutions with various W concentrations were spun on SiO_2/p$^+$-Si substrates to construct bottom-gate/top-contact TFTs. The resulting thin films were annealed at 240 ^{o}C ~ 330 ^{o}C. The amorphous nature of all the thin films was confirmed by XRD measurements (Fig. S1, ESI†). In addition, there is no significant difference in the root-mean square (RMS) surface roughness among these thin films as investigated by AFM (Fig. S2, ESI†), which is found to be ~ 0.2 nm. The results indicate that the differences in crystalline structures and morphologies will not affect the electrical performance.

Fig. 3(a)-(c) show the representative transfer characteristics for TFTs based on IWO-1, IWO-3, and IWO-5 channel layers, respectively. The TFT performance parameters, including carrier mobility μ_{sat}, V_{TH}, on/off current ratio (I_{on}/I_{off}), and the *SS*, are summarized in Table 1. It is found that the IWO TFTs were active at a low annealing temperature of 240 ^{o}C, independent of W concentration. With the increase of the annealing temperature, the continuous increase in μ_{sat} and the negative shift in V_{TH} are observed. For solution-processed metal-oxide semiconductor thin films, the thermally-driven condensation processes accelerate the conversion from metal hydroxides into the oxides. The degree of metal-oxide bonds formation and oxygen-vacancy generation rely primarily on the annealing temperature.[12, 38-41] In our recent reports, it was found that the dehydroxylation reaction at high annealing temperature could lead to the creation of charge carriers in the channel layers.[15, 16] It's known that

the carrier transport in semiconductor films is governed by percolation conduction over trap states and is enhanced at high carrier concentrations by filling the trap states.[42] The field-effect mobility of the semiconductor channel layers together with the electrical performance of as-integrated TFTs depend on the carrier concentration. As a result, this will not only increase the saturation current but also enhance the μ_{sat} value of the TFTs, which is consistent with the phenomena observed in this study.
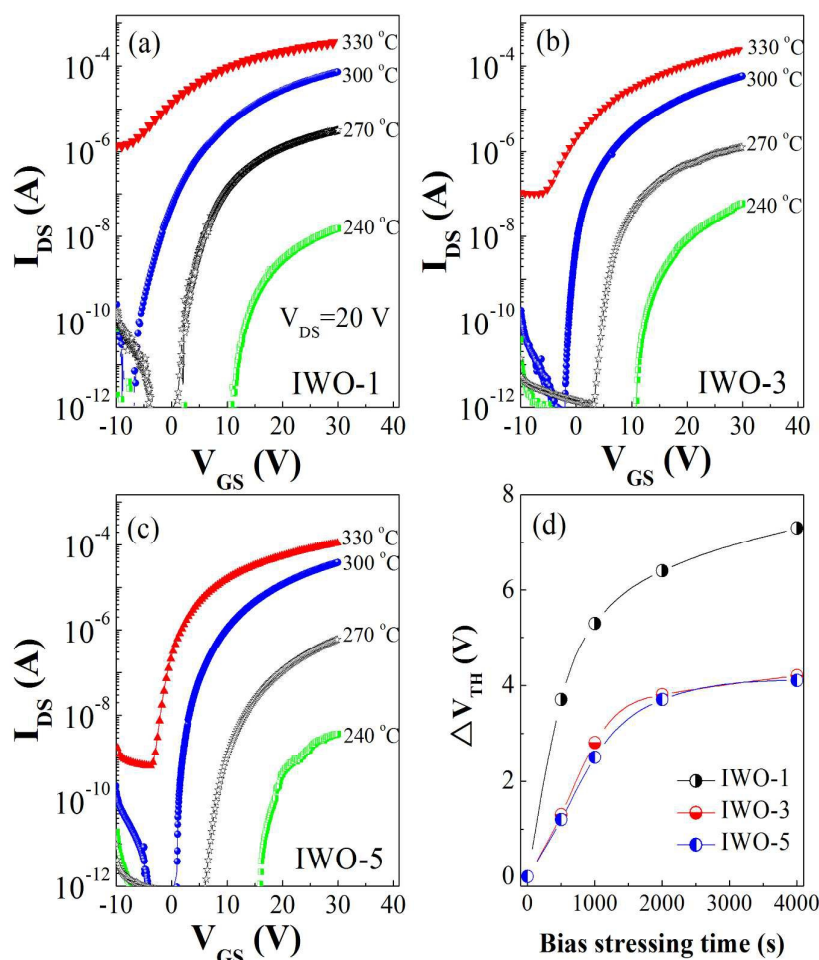
Fig. 3 Transfer characteristics of (a) IWO-1, (b) IWO-3, and (c) IWO-5 TFTs annealed at indicated temperatures. (d) Threshold voltage shift ΔV_{TH} as a function of stress time for various IWO TFTs annealed at 300 ^{o}C.

For 300 ^{o}C-annealed IWO TFTs, the turn-on voltage (V_{on}) shifted in a positive direction to $\sim$ 0 V with increasing W concentration from 1% to 5%. Usually, a normally-off operation (the drain current is in the off region when no gate voltage applied) is required in devices with low power consumption, a V_{on} of $\sim$ 0 V is indispensable. Meanwhile, the saturation current was found to decrease gradually

from 80 μA to 30 μA, which infer a decrease in the μ_{sat} from 4.1 to 2.2 cm^2/Vs. Because the W element acts as the carrier suppressor in IWO system, it is reasonable that the μ_{FE} and the output current are deteriorated with increasing W content. In addition, the swing performance was improved from 2.2 V/dec (IWO-1 TFT) to 0.7 V/dec (IWO-5 TFT). This is mainly attributed to the reduction in electron concentration and the sub-gap states in the vicinity of the Femi-level.[43]

Since the TFT is the basic unit of integrated circuit, the operational stability of the TFT is one of the most important aspects when considering display applications such as the backplane of AMLCDs and AMOLEDs. To further demonstrate the reliability of these solution-processed IWO channel layers, the bias stability measurements of the TFT devices were carried out. The transfer characteristics of the TFTs using channel layers of IWO-1, IWO-3, and IWO-5 under positive bias stress (PBS, V_G = 30 V) tests are shown in Fig. S3 (ESI†). The variations of the threshold voltage shift (ΔV_{TH}) as a function of stress time are summarized in Fig. 3d. The parallel V_{TH} shift of the transfer curve, with a negligible change in the *SS* value, is attributed to the charge trapping at IWO/SiO$_2$ interface.[44] Besides, the absorption of oxygen on the IWO back channel can also lead to V_{TH} instability under PBS test. When PBS is applied under atmospheric conditions, the surrounding oxygen molecules with large electronegativity can capture electrons from the conduction band to form O^{2-} species. This can deplete the carriers in the IWO channel layer, leading to a positive ΔV_{TH}.[45] The resulting band diagram is shown in Fig. S4 (ESI†).

Table 1. Performance comparison of IWO TFTs estimated from the transfer characteristics presented in Fig. 3(a)-(c).

Sample	Temperature [°C]	μ_{sat} [cm^2/Vs]	V_{TH} [V]	*SS* [V/dec]	I_{on}/I_{off}
IWO-1	240	--	12.2±1.1	1.1±0.1	~10^5
	270	~0.2	5.0±0.9	1.2±0.1	10^6-10^7
	300	4.1±0.2	4.2±0.7	2.2±0.2	10^7-10^8
	330	7.7±0.5	-6.2±0.7	8.5±0.3	10^2-10^3
IWO-3	240	--	13.6±0.8	1.0±0.1	~10^5
	270	~0.1	6.4±0.7	0.8±0.1	~10^6
	300	3.4±0.2	5.1±0.5	0.8±0.1	10^7-10^8
	330	7.1±0.4	-2.0±0.4	4.2±0.3	10^3-10^4
IWO-5	240	--	16.3±0.8	1.1±0.1	10^4-10^5
	270	~0.1	13.0±0.6	1.1±0.1	10^6-10^7
	300	2.2±0.1	7.4±0.5	0.7±0.2	10^7-10^8
	330	6.5±0.4	-0.8±0.2	1.3±0.1	~10^5

After 4000 s bias stressing, it was found that the TFTs with channel layers of IWO-3 and IWO-5 had a smaller ΔV_{TH} values (~4.0 V) compared to the IWO-1 TFT (7.3 V). It is known that the oxygen vacancy acts as deep donor defects in oxide semiconducting materials. The W dopant is expected to suppress the formation of excess oxygen vacancies due to the high oxygen bond-dissociation energy of W (720 kJ/mol).[6] As a result, with the incorporation of WO_3, the trap states originating from the oxygen vacancies decreased and the bias stability of the TFT was improved. Meanwhile, the N_s^{max} values of the IWO-1, IWO-3, and IWO-5 TFTs were calculated to be 3.21×10^{12}, 1.05×10^{12}, 0.93×10^{12} cm^{-2} according to equation 2 (see experimental). The reduction in N_s^{max} indicates that the interfacial states between IWO/SiO$_2$ were improved with increasing W concentration, which agrees well with the variation of the ΔV_{TH} under bias stress measurement.

Overall consideration the electrical performance of the IWO TFTs, it can be concluded that the IWO system with 3% WO_3 dopant concentration is the optimized composition. The IWO TFT with optimized composition not only provides high electrical performance, but also exhibits an acceptable bias stability. However, all these devices operate at high voltages (≥ 30 V) and hence consume much more power. This is primarily due to the 200-nm-thick SiO_2 gate dielectric employed and its relatively low dielectric constant (~3.9). In order to decrease the operating voltage, and hence reduce the overall power consumption of the IWO TFTs, the SiO_2 dielectric layer was replaced by a WI high-k AlO_x dielectric. The entire dielectric deposition process was performed at a moderate temperature of 350 ^{o}C in a green route. As shown in Fig. 4a, the AlO_x thin film exhibits an amorphous nature and a smooth surface with an RMS value of 0.16 nm. Amorphous dielectric material is preferred because grain boundaries usually act as preferential paths for impurity diffusion and leakage current, resulting in an inferior dielectric performance. Besides, the smooth surface of the gate dielectric can suppress the surface-roughness-induced leakage current and achieve expeditious carrier transport in the channel.[46] To characterize the electrical properties of the AlO_x thin film, the Al/AlO_x/p$^+$-Si capacitor was fabricated. As shown in Fig. 4b, the areal capacitance of the AlO_x dielectric is found to be 420 nF/cm^2 at 20 Hz with a relative dielectric constant of 7. The breakdown analysis shows that the AlO_x dielectric thin film exhibits reliable breakdown characteristics at an electrical field of 5 MV/cm, where the leakage current

density (J_{leak}) was lower than 0.1 $\mu A/cm^2$. The J_{leak} at 1 MV/cm was 0.4 nA/cm^2, which is sufficiently low to be applied in TFTs as a gate dielectric compared to the conventional SiO_2 dielectric ($J_{leak(SiO2)}$~0.3 nA/cm^2).[47]
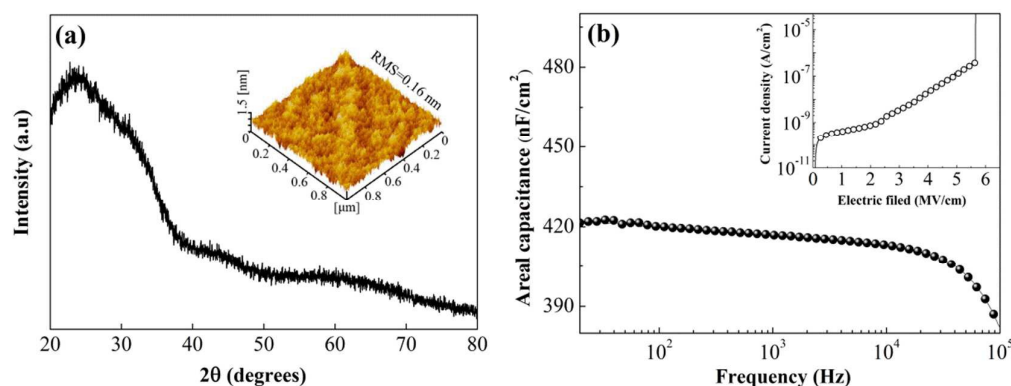
Fig. 4 (a) XRD pattern and AFM image of the WI AlO_x thin film. (b) Areal capacitance of an $Al/AlO_x/p^+$-Si capacitor at various frequencies. The leakage-current density versus electric field is shown in the inset.

With the successful fabrication of high-quality amorphous AlO_x dielectric thin film, the fully solution-processed IWO/AlO_x TFT was integrated by fabricating the IWO-3 thin film on AlO_x dielectric layer. Fig. 5a and b show the output and transfer curves of as-fabricated IWO/AlO_x TFT. The device exhibits typical n-channel behavior with clear pinch-off and current saturation. In addition, the TFT represents high electrical performances, including a high μ_{sat} of 15.3 cm^2/Vs, a low V_{TH} of 0.37 V, an I_{on}/I_{off} of 5×10^7, a small SS value of 68 mV dec^{-1}, and a low operating voltage of 2 V. As a result, the TFT device consumes much lower power compared to the SiO_2-based IWO TFTs (Fig. 3), which is critical for low-consumption electronics. Particularly, the SS value (68 mV/dec) is close to the theoretical limit (60 mV/dec),[48] indicating an electronic-clean IWO/AlO_x interface. From SS value, the N_s^{max} at IWO/AlO_x interface was calculated to be 4.4×10^{11} cm^{-2}. This value is much smaller than the TFTs based on CVD AlO_x (2.7×10^{12} cm^{-2}),[49] anodic Al_2O_3 (1.2×10^{12} cm^{-2}),[50] sputtered AlO_x (1.1×10^{13} cm^{-2}),[51] and organic-based spin-coated[25] AlO_x (1.1×10^{12} cm^{-2}) dielectrics. Such a small N_s^{max} is not only beneficial to carrier transport in the interface region, but also to the operational stability. To investigate the bias stability of the solution-processed IWO/AlO_x TFT, the PBS test was carried out by applying a constant gate voltage of 2 V. The device was stressed for 7200 s and the results are shown in Fig. 5c. The as-fabricated TFT showed a small ΔV_{TH} of ~ 0.15 V without changing the SS value. Compared with SiO_2-based IWO TFT, a small variation of

ΔV_{TH} indicates that few defects were observed at the IWO/AlO$_x$ interface, which is consistent with the N_s^{max} investigation.
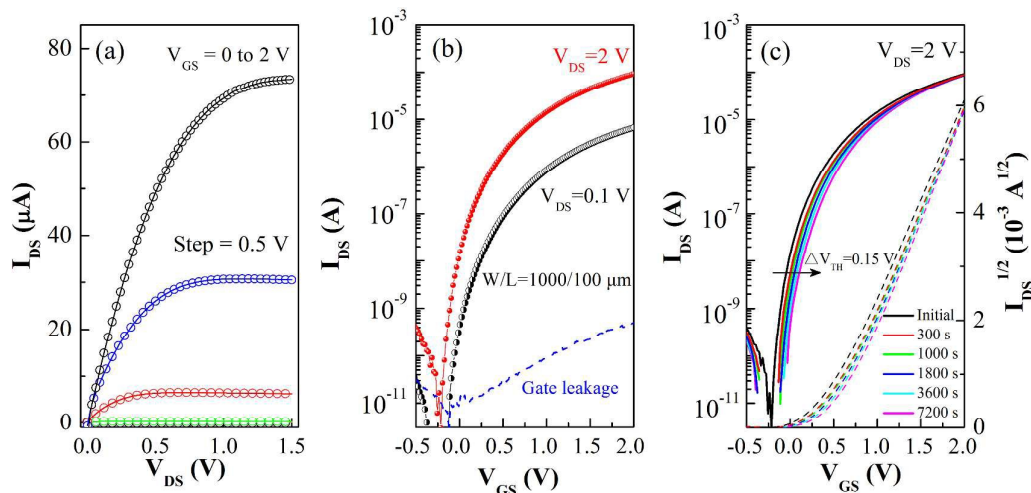
Fig. 5 (a) Output and (b) transfer characteristics of solution-processed IWO/AlO$_x$ TFT. (c) Transfer curves of IWO/AlO$_x$ TFT under PBS test for a duration of 7200 s.

Usually, the TFTs were operated at a constant voltage, and the capacitance value at a relatively low frequency was often adopted to calculate device mobility. In this report the areal capacitance of 420 nF/cm^2 (20 Hz) was used to eliminate mobility overestimation.[46] By replacing SiO$_2$ with AlO$_x$ dielectric, the μ_{sat} was significantly enhanced by a factor of 4.5. This increase in the μ_{sat} is beneficial from the electronic-clean interface and high capacitance density of the AlO$_x$ dielectric. Based on the multiple-trap-and-release (MTR) model, Lee *et al.*[52] recently proposed that a higher carrier mobility can result from an increased gate capacitance (i.e. increased charge) stemming from the higher dielectric constant of the gate dielectric relative to SiO$_2$. It is known that the electron transport in the amorphous n-type oxide channel layer is governed by hopping conduction between neighboring cation ions (Fig. 6a).[3] Before participating the transport in the conduction band, the induced electrons need to fill the localized states between the energy gaps (Fig. 6b). By integrating the channel layer with a dielectric with large capacitance, a large amount of induced electrons quickly filled the lower-lying localized states. Then, the additionally accumulated electrons could occupy the upper-lying localized states. As a result, the electrons could jump to the neighboring localized states easily, along the percolating-conduction path, which leads to an enhanced electron mobility.[53] In this work, the IWO thin films were achieved by solution process and the IWO TFTs were integrated

for the first time. Further studies on the etching rates of IWO films with various W concentrations or the integration on flexible substrate by using DUV photochemical activation technique[14] are more attractive and are currently ongoing.
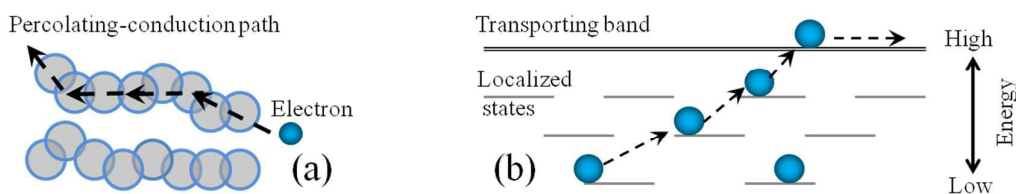
Fig. 6 (a) Schematic of electron-transporting mode and (b) energy-band diagram in n-type amorphous oxide semiconductor.

4. CONCLUSIONS

In this work, an eco-friendly solution process was applied to fabricate amorphous IWO semiconductor thin films and the TFT devices. The electrical performances of IWO TFTs, together with the structural and morphological characteristics of IWO thin films, were systematically investigated as functions of the W doping concentration and annealing temperature. The IWO thin film remained amorphous up to an annealing temperature of 330 $^{\circ}$C and exhibited smooth surface (RMS $\approx$ 0.2 nm). The 300 $^{\circ}$C-annealed IWO-3 TFT exhibited the highest electrical performance, including a μ_{sat} of 3.4 cm^2/V·s, an *SS* value of 0.8 V/dec, a V_{on} ~0 V, and an I_{on}/I_{off} of ~10^8, respectively. Furthermore, the fully solution-processed IWO TFT based on WI-AlO$_x$ gate dielectric was successfully demonstrated to exhibit a high μ_{sat} of 15.3 cm^2/Vs at a low operating voltage of 2 V. This work paves the way for the development of solution-processed IWO films in a range of applications that span beyond TFT devices. Besides, this eco-friendly fabrication technique provides a new approach to integrate more amorphous oxide materials into low-cost, low-power consumption, and large-area electronic and biologic detecting electronics.

Electronic Supplementary information

Fig. S1 shows the XRD patterns for IWO thin films as a function of W content annealed at 330 $^{\circ}$C. Fig. S2 shows the AFM patterns of IWO thin films annealed at various temperatures. Fig. S3 shows the variation in the transfer characteristics of TFTs fabricated using IWO-1, IWO-3, and IWO-5 films under the PBS condition for the duration of 4000 s. Fig. S4 shows energy band diagrams of the IWO TFT under PBS test in air.

Corresponding author

*E-mail: gxliu@qdu.edu.cn; fukaishan@yahoo.com;

Notes

The authors declare no competing financial interest.

References

1 E. Fortunato, P. Barquinha, R. Martins, *Adv. Mater.*, 2012, **24**, 2945.

2 A. Facchetti, T. J. Marks, Transparent electronics, From Synthesis to Applications, Wiley, Chichester, UK, 2010.

3 K. Nomura, H. Ohta, A. Takagi, T. Kamiya, M. Hirano, H. Hosono, *Nature*, 2004, **432**, 488.

4 S. Aikawa, P. Darmawan, K. Yanagisawa, T. Nabatame, Y. Abe, K. Tsukagoshi, *Appl. Phys. Lett.*, 2013, **102**, 102101.

5 M. Kim, J. H. Jeong, H. J. Lee, T. K. Ahn, H. S. Shin, J. S. Park, J. K. Jeong, Y. G. Mo, H. D. Kim, *Appl. Phys. Lett.*, 2007, **90**, 212114.

6 T. Kizu, S. Aikawa, N. Mitoma, M. Shimizu, X. Gao, M. F. Lin, T. Nabatame, K. Tsukagoshi, *Appl. Phys. Lett.*, 2014, **104**, 152103.

7 L. T. Yan, R. E. I. Schropp, *Thin Solid Films*, 2012, **520**, 2096.

8 R. K. Gupta, K. Ghosh, P. K. Kahol, *Appl. Surf. Sci.*, 2009, **255**, 8926.

9 K. Tsukagoshi, J. Tanabe, I. Yagi, K. Shigeto, K. Yanagisawa, Y. Aoyagi, *J. Appl. Phys.*, 2006, **99**, 064506.

10 Z. Hu, J. Zhang, X. Chen, S. Ren, Z. Hao, X. Geng, Y. Zhao, *Sol. Energ. Mat. Sol. C.*, 2011, **95**, 2173.

11 K. Banger, Y. Yamashita, K. Mori, R. Peterson, T. Leedham, J. Rickard, H. Sirringhaus, *Nat. Mater.*, 2010, **10**, 45.

12 M. G. Kim, M. G. Kanatzidis, A. Facchetti, T. J. Marks, *Nat. Mater.*, 2011, **10**, 382.

13 T. Jun, K. Song, Y. Jeong, K. Woo, D. Kim, C. Bae, J. Moon, *J. Mater. Chem.*, 2011, **21**, 1102.

14 Y. H. Kim, J. S. Heo, T. H. Kim, S. Park, M. H. Yoon, J. Kim, M. S. Oh, G. R. Yi, Y. Y. Noh, S. K. Park, *Nature*, 2012, **489**, 128.

15 A. Liu, G. X. Liu, H. H. Zhu, F. Xu, E. Fortunato, R. Martins, F.K. Shan, *ACS Appl. Mater. Interfaces*, 2014, **6**, 17364.

16 G. X. Liu, A. Liu, H. H. Zhu, B. C. Shin, E. Fortunato, R. Martins, Y. Q. Wang, F. K. Shan, *Adv. Funct. Mater.*, 2015, **25**, 2564.

17 Y. S. Rim, H. Chen, X. Kou, H.-S. Duan, H. Zhou, M. Cai, H. J. Kim, Y. Yang, *Adv. Mater.*, 2014, **26**, 4273.

18 R. Branquinho, D. Salgueiro, L. Santos, P. Barquinha, L. Pereira, R. Martins, E. Fortunato, *ACS Appl. Mater. Interfaces*, 2014, **6**, 19592.

19 Y. H. Lin, H. Faber, K. Zhao, Q. Wang, A. Amassian, M. McLachlan, T. D. Anthopoulos, *Adv. Mater.*, 2013, **25**, 4340.

20 C. Avis, J. Jang, *J. Mater. Chem.*, 2011, **21**, 10649.

21 C. Avis, Y. G. Kim, J. Jang, *J. Mater. Chem.*, 2012, **22**, 17415.

22 G. Adamopoulos, S. Thomas, P. H. Wöbkenberg, D. D. C. Bradley, M. A. McLachlan, T. D. Anthopoulos, *Adv. Mater.*, 2011, **23**, 1894.

23 K. Song, W. Yang, Y. Jung, S. Jeong, J. Moon, *J. Mater. Chem.*, 2012, **22**, 21265.

24 C. Avis, H. R. Hwang, J. Jang, *ACS Appl. Mater. Interfaces*, 2014, **6**, 10941.

25 W. Xu, H. Wang, L. Ye, J. Xu, *J. Mater. Chem. C*, 2014, **2**, 5389.

26 P. K. Nayak, M. Hedhili, D. Cha, H. Alshareef, *Appl. Phys. Lett.*, 2013, **103**, 033518.

27 G. Adamopoulos, S. Thomas, D.D. Bradley, M.A. McLachlan, T.D. Anthopoulos, *Appl. Phys. Lett.*, 2011, **98**, 123503.

28 G. Huang, L. Duan, G. Dong, D. Zhang, Y. Qiu, *ACS Appl. Mater. Interfaces*, 2014, **6**, 20786.

29 T. Jun, Y. Jung, K. Song, J. Moon, *ACS Appl. Mater. Interfaces*, 2011, **3**, 774.

30 S. Y. Je, B. G. Son, H. G. Kim, M. Y. Park, L. M. Do, R. Choi, J. K. Jeong, *ACS Appl. Mater. Interfaces*, 2014, **6**, 18693.

31 Y. Choi, G. H. Kim, W. H. Jeong, J. H. Bae, H. J. Kim, J. M. Hong, J. W. Yu, *Appl. Phys. Lett.*, 2010, **97**, 162102.

32 H. Li, M. Qu, Q. Zhang, *IEEE Electron Device Lett.*, 2013, **34**, 1268.

33 C. J. Kim, S. Kim, J. H. Lee, J. S. Park, S. Kim, J. Park, E. Lee, J. Lee, Y. Park, J. H. Kim, *Appl. Phys. Lett.*, 2009, **95**, 252103.

34 J. W. Hennek, J. Smith, A. Yan, M. G. Kim, W. Zhao, V. P. Dravid, A. Facchetti, T. J. Marks, *J. Am. Chem. Soc.*, 2013, **135**, 10729.

35 Y. Zhang, *Inorg. Chem.*, 1982, **21**, 3886.

36 S. Parthiban, J. Y. Kwon, *J. Mater. Res.*, 2014, **29**, 1585.

37 K. Choi, M. Kim, S. Chang, T. Y. Oh, S. W. Jeong, H. J. Ha, B. K. Ju, Jpn. *J. Appl. Phys.*, 2013, **52**, 060204.

38 T. Kamiya, K. Nomura, H. Hosono, *J. Disp. Technol.*, 2009, **5**, 468.

39 J. S. Lee, Y. J. Kwack, W. S. Choi, *ACS Appl. Mater. Interfaces*, 2013, **5**, 11578.

40 Y. H. Hwang, J. S. Seo, J. M. Yun, H. Park, S. Yang, S. H. K. Park, B. S. Bae, *NPG Asia Mater.*, 2013, **5**, e45.

41 S. Jeong, J. Y. Lee, S. S. Lee, Y. Choi, B. H. Ryu, *J. Phys. Chem. C*, 2011, **115**, 11773.

42 S. Jeong, Y.G. Ha, J. Moon, A. Facchetti, T. J. Marks, *Adv. Mater.*, 2010, **22**, 1346.

43 H. Park, Y. Nam, J. Jin, B. S. Bae, *J. Mater. Chem. C*, 2014, **2**, 5998.

44 T. M. Pan, C. H. Chen, J. H. Liu, J. L. Her, K. Koyama, *IEEE Electron Device Lett.*, 2014, **35**, 66.

45 Y. H. Hwang, H. G. Im, H. Park, Y. Y. Nam, B. S. Bae, *ECS J. Solid State Sci. Technol.*, 2013, **2**, Q200.

46 W. Xu, H. Wang, F. Xie, J. Chen, H. Cao, J. B. Xu, *ACS Appl. Mater. Interfaces*, 2015, **7**, 5803.

47 K. M. Kim, C. W. Kim, J. S. Heo, H. Na, J. E. Lee, C. B. Park, J. U. Bae, C. D. Kim, M. Jun, Y. K. Hwang, *Appl. Phys. Lett.*, 2011, **99**, 242109.

48 M. Lorenz, H. von Wenckstern, M. Grundmann, *Adv. Mater.*, 2011, **23**, 5383.

49 M. Furuta, T. Kawaharamura, D. Wang, T. Toda, T. Hirao, *IEEE Electron Device Lett.*, 2012, **33**, 851.

50 L. Lan, J. Peng, *IEEE Trans. Electron Devices*, 2011, **58**, 1452.

51 J. Li, F. Zhou, H. P. Lin, W. Q. Zhu, J. H. Zhang, X. Y. Jiang, Z. L. Zhang, *Curr. Appl. Phys.*, 2012, **12**, 1288.

52 E. Lee, J. Ko, K. H. Lim, K Kim, S. Y. Park, J. M. Myoung, Y. S. Kim, *Adv. Funct. Mater.*, 2014, **24**, 4689.

53 A. Liu, G. X. Liu, H. H. Zhu, Huijun Song, B. C. Shin, E. Fortunato, R. Martins, F. K. Shan, *Adv. Funct. Mater.*, 2015, **25**, 7180.

Table of Contents (TOC)

Eco-friendly IWO thin films are fabricated via low-cost solution process and employed as channel layers in thin-film transistors.